RSC Advances

PAPER

View Article Online
View Journal | View Issue

Cite this: *RSC Adv.*, 2017, **7**, 6202

Tuning optical band gap by electrochemical reduction in TiO_2 nanorods for improving photocatalytic activities†

Jong-Won Yun,[a] Ki Yeon Ryu,[a] Tri Khoa Nguyen,[a] Farman Ullah,[a] Yun Chang Park[b] and Yong Soo Kim*[a]

Received 15th October 2016
Accepted 2nd January 2017

DOI: 10.1039/c6ra25274e

www.rsc.org/advances

In this study, we investigate the tuning of the optical band gap of TiO_2 nanorods (TiO_2 NRs) by electrochemical methods for improving their photocatalytic activities. A seed layer prepared by RF-magnetron sputtering is employed to increase the adhesion between TiO_2 NRs and substrate to prevent the peel-off of TiO_2 NRs from substrate during electrochemical reduction process. The morphological study shows the stability of TiO_2 NRs structure after reduction process. The electrochemical reduction process increased the amount of Ti^{3+} (a reduced state of Ti^{4+}) and oxygen vacancy by 2.2% and 3.6%, respectively. The process also tune the optical band of TiO_2 NRs from 3.0 eV to 2.84 eV due to the up-shift of valence band to Fermi level. The reduced band gap of NRs improve the photocatalytic activities by 1.48 times due the increase of its absorbance range from UV to visible in solar spectrum. The photocatalytic activities were 24.3 times improved by depositing a ultrathin layer of Pt as electron collector.

Introduction

Its excellent chemical stability, nontoxicity, catalytic activity and low cost make TiO_2 an attractive photocatalytic material for a range of applications, such as water purification, self-cleaning, and solar energy conversion.[1–4] On the other hand, the use of TiO_2 in the visible region is limited by its large energy band gap. In recent years, significant effort has been devoted to improving the visible absorbance of TiO_2 to enhance its photocatalytic activity in solar light.[5–19]

A well-known approach is hetero-doped TiO_2 using impurity cations, Cr, Ag, *etc.*, and anions, N, F, C, *etc.*[6,9–12] Nitrogen-doped TiO_2 may produce sub-levels by hybridization of the N 2p and O 2p states near the valence band of TiO_2 that would improve the visible light activity.[12] On the other hand, it can produce carrier recombination centers that may reduce the catalytic activity in the UV region.[20–23] Self-doped TiO_2 is a useful method for improving the photocatalytic activities of TiO_2 in the UV-Vis region by generating a sub-band level in the TiO_2 band gap and not involving structure defects.[24–29] Naldoni *et al.* reported that the reduced band gap of Ti^{3+} self-doped TiO_2 results from the slight up-shift of the valence band (VB) to the Fermi level.[21] Kang *et al.* also reported the same behavior of the up-shift of VB.[30] Moreover, the oxygen vacancies (V_O) formed during Ti^{3+} self-doping increase the carrier density and charge transfer.[31] Well-known approach could be the thermal annealing method used famously for Ti^{3+} self-doped TiO_2;[32–36] however, it require a carrier gas and control system for temperature and pressure. Recently, an electrochemical reduction method has been adopted widely because of its simple mechanism, low cost and fast self-doping properties. On the other hand, owing to the lattice mismatch between rutile TiO_2 and the substrate,[37] electrochemical self-doped approach is only employed in TiO_2 nanotubes anodized from Ti-foil.[30,38–40]

In this study, the electrochemical reduction method was used to self-dope Ti^{3+} into TiO_2 nanorods (TiO_2 NRs) grown on a FTO substrate for optical band gap tuning. To prevent the peel-off of TiO_2 NRs from the substrate due to large lattice mismatch, a TiO_2 seed layer was introduced by RF-magnetron sputtering to enhance the adhesion between TiO_2 and FTO substrate. X-ray photoelectron spectroscopy and UV-Vis spectroscopy were employed to examine the tuning of the TiO_2 optical band gap. In a study of photocatalysis, the reduced TiO_2 nanorods ($rTiO_2$ NRs) exhibited better performance compared to the as-grown TiO_2 NRs. The photocatalytic activities of $rTiO_2$ NRs were enhanced significantly by decorating an ultrathin layer of Pt on the $rTiO_2$ NRs as an electron collector by RF magnetron sputtering.

Experiment

Synthesis of TiO_2 nanorods

Prior to synthesis, FTO substrate (F:SnO_2, Tec 20, 8 Ω $\square^{-1}$) was cleaned by immersing in a mixture of DI water, acetone and 2-

[a]*Department of Physics, Energy Harvest-Storage Research Center, University of Ulsan, Ulsan 44610, South Korea. E-mail: yskim2@ulsan.ac.kr*

[b]*Measurement and Analysis Division, National Nanofab Center, Daejeon 34141, South Korea*

† Electronic supplementary information (ESI) available. See DOI: 10.1039/c6ra25274e

propanol (1 : 1 : 1 of volume ratio) and ultra-sonicated for 30 min. TiO_2 seed layer was deposited on FTO substrate using RF-magnetron sputtering (details in Table S1†). To synthesize TiO_2 NRs by hydrothermal method, 0.65 mL of titanium(IV) *n*-butoxide (TBO, Aldrich Chemicals, 97%), 25 mL of HCl 38%, and 25 mL of DI water were mixed and stirred for 30 min.

RF-deposited TiO_2 seed layer on FTO substrate was placed face side down in the grown solution in a Teflon beaker. To grow the TiO_2 NRs, the Teflon beaker was then sealed in a stainless steel auto-clave at 165 °C for 10 h. The as-grown TiO_2 NRs were washed with DI water and ethanol, and then annealed at 450 °C for 60 min. To compare the quality of RF-sputtered seed layer, another TiO_2 NRs were also grown on a seed layer prepared by sol–gel method. The seed layer was prepared by spin coating of TiO_2 polymeric solution.[41,42]

Electrochemical reduction of TiO_2 NRs and Pt decoration

The synthesized TiO_2 NRs were reduced using an electrochemical reduction method; connecting TiO_2 NRs/FTO (working electrode) and a Pt wire (counter electrode, 1 mm of diameter and 9 cm of length, 99.95%). Electrochemical reduction process was done in a 0.1 M of NaOH electrolyte with negative bias, −3 V *vs.* Pt for 5 to 20 min. The final $rTiO_2$ NRs were washed in DI water, and dried with dry N_2. To improve photocatalytic activities, an ultrathin layer of Pt as electron collector was deposited on surface of the $rTiO_2$ NRs by using a RF-magnetron sputtering at 30 W for 2 min (details in Table S1†).

Characterization

The morphology and crystallinity of the TiO_2 NRs and $rTiO_2$ NRs were studied using field emission scanning electron microscopy (FE-SEM, JEOL, JSM 7600F) and a transmission electron microscope (FE-TEM, JEI, Tecnai G2F30 S-Twin). The crystalline structure was characterized by a X-ray diffraction (XRD, RIGAKU, D/MAX 2500-V/PC, using Cu Kα radiation, λ = 1.540598 Å). X-ray photoelectron spectroscopy (XPS) using a Leybold spectrometer with an Al Kα monochromatic beam (1486.6 eV, ESCALAB250, Theta Probe XPS system) and ultraviolet photoelectron spectroscopy (UPS) study with a He(I) beam source (21.21 eV) was done. UV-Vis spectra were recorded using an optical spectrophotometer (Varian, Cary 5000).

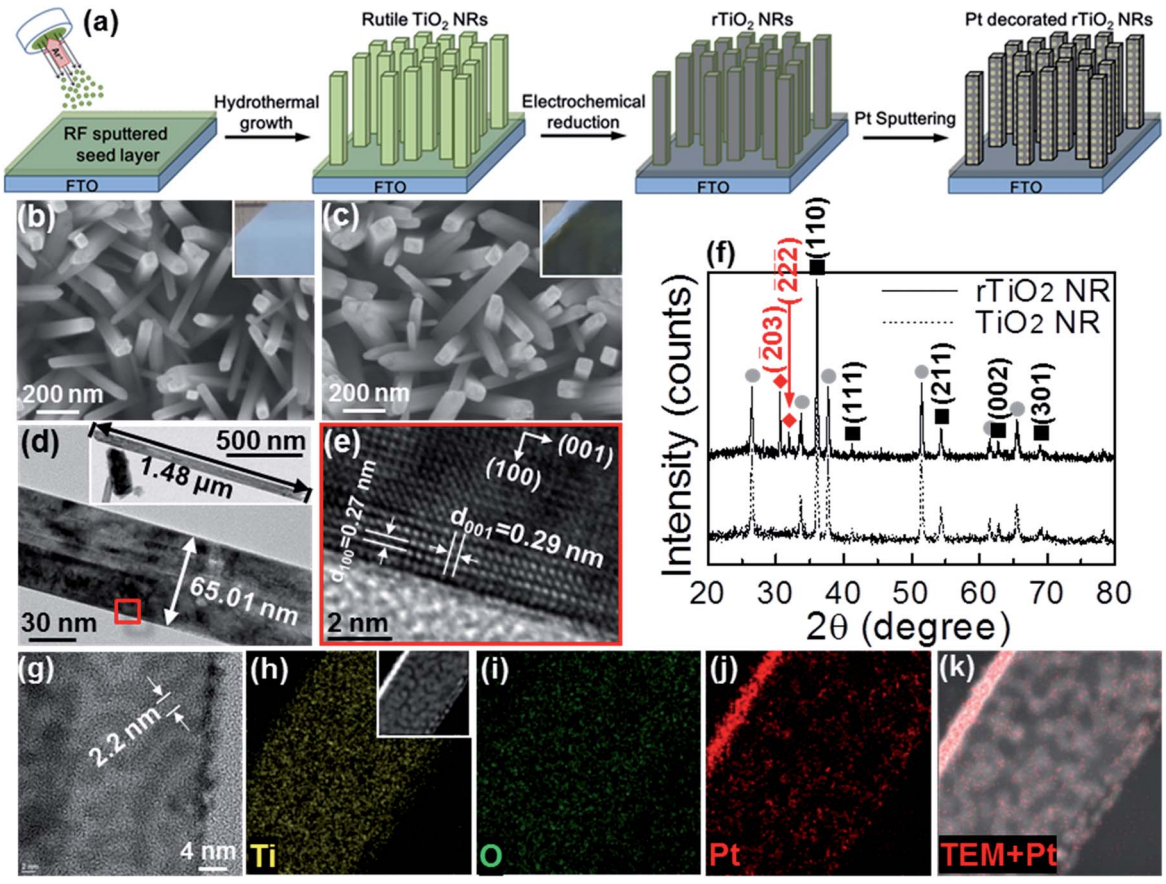

Fig. 1 (a) Schematic diagram of experimental sequence. (b and c) FE-SEM images of (b) TiO_2 NRs and (c) $rTiO_2$ NRs (insets: photograph image of (b) TiO_2 NRs and (c) $rTiO_2$ NRs on FTO substrate, indicating that the TiO_2 NRs was changed from white to dark brown after the reducing process while the morphology was stable). (d) TEM (inset: a low-magnification image) and (e) HR-TEM image of TiO_2 NRs grown along the [001] direction with an average length of 1.5 μm and diameter of 65 nm. (f) XRD result of TiO_2 NRs and $rTiO_2$ NRs. Two peaks are appeared at 30.64° and 31.96° 2θ after electrochemical reduction by the formation of V_O. (g) TEM image and (h–k) EDS mapping images of the ultrathin Pt decorated $rTiO_2$ NRs. The inset in (h) shows Pt decorated $rTiO_2$ NRs used EDS mapping.

Photocatalytic activities measurement

Photocatalytic performances of the TiO_2 NRs, $rTiO_2$ NRs and Pt decorated rTO_2 NRs were evaluated by photo-degradation of 15 mL of 15 μM methylene blue (MB, $C_{16}H_{18}N_3SCl$) under Xe-lamp irradiation. The intensity of the light source was calibrated with a standard Si-photodiode detector of a KG-3 filter (Newport Co., Oriel) to AM 1.5G illumination of 100 mW cm^{-2}. Photocatalytic degradation of MB was determined from the absorbance of MB solution at 665 nm using a UV-Vis spectrophotometer.

Results and discussion

Fig. 1(a) shows schematically the growth process of TiO_2 NRs, $rTiO_2$ NRs and Pt decorated $rTiO_2$ NRs on a RF-magnetron sputtered TiO_2 seed layer/FTO substrate. The RF-sputtered TiO_2 seed layer plays an important role in enhancing the adhesion between the grown TiO_2 NRs and substrate. The insets in Fig. 1(b) and (c) show photographs of the TiO_2 NRs before and after reduction, respectively. The TiO_2 NRs has maintained their quality, indicating the good adhesion between the TiO_2 NRs and substrate. On the other hand, the $rTiO_2$ NRs on sol–gel TiO_2 seed layer show poor adhesion as compared to those on the RF-magnetron sputtered seed layer (Fig. S1†). Moreover, the RF-sputtered seed layer exhibited higher mechanical durability as compared to sol–gel.[43,44] To check the adhesion more closely, the sample was analyzed by FE-SEM before and after the reduction process, as depicted in Fig. 1(b) and (c), respectively. The TiO_2 NRs preserved their quality, which further confirmed the excellent adhesion between TiO_2 NRs and substrate.

The TEM image in Fig. 1(d) shows that the TiO_2 NRs are approximately 1.5 μm in length and 65 nm in diameter. The HR-TEM image shown in Fig. 1(e) taken at the highlighted region in Fig. 1(d) shows that the growth direction of TiO_2 NR is along the (001) direction, which confirms the typical TiO_2 NR structure. This observation is similar to previous reports.[45] Fig. 1(f) show the XRD results of the TiO_2 NRs and $rTiO_2$ NRs. The diffraction peaks at 26.42°, 33.68°, 37.68°, 51.46°, 61.54° and 65.46° 2θ (gray circles) correspond to the crystalline structure of the FTO substrate (S.G. $P4_2/mnm$, JCPDS no. 00-046-1088, $a = b = 0.4750$ nm, $c = 0.3198$ nm). The XRD peaks at 36.04°, 41.22°, 54.30°, 62.70° and 68.92° 2θ (dark squares) are consistent with the tetragonal rutile phase of TiO_2 (S.G. $P4_2/mnm$, JCPDS no. 01-070-7347, $a = b = 0.4593$ nm and $c = 0.2961$ nm).[46] The rutile structure has a 4_2 screw axis along the c-axis; hence, the domination of (110) faces indicates the promoted growth of the TiO_2 NR along the (001) direction.[47–49] After electrochemical reduction, two XRD peaks (red diamonds) are appeared at 30.64° and 31.96° 2θ which match to the $(\bar{2}03)$ and $(\overline{222})$ faces of Ti_4O_7 (S.G. $P1$, JCPDS no. 77-1390) lacking oxygen atoms. This shows that the electrochemical process is suitable for generating oxygen vacancies (V_O) in $rTiO_2$ NRs. Owing to the lower band gap of $rTiO_2$ NRs as

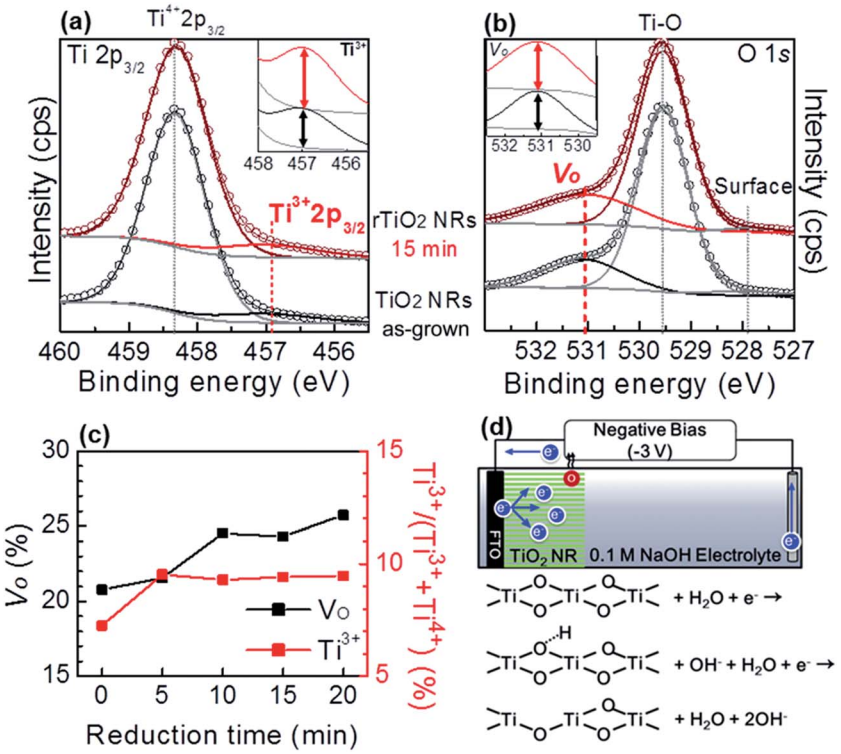

Fig. 2 XPS core levels spectra of (a) Ti $2p^{3/2}$ and (b) O 1s of TiO_2 NRs and $rTiO_2$ NRs (inset: magnification graph of (a) Ti^{3+} peak and (b) V_O peak). (c) Time dependent proportion change of V_O and Ti^{3+} obtained from deconvolution of XPS results. Ti^{3+} content is likely to saturate at a mean value of 9.4% after 5 min of reduction time, V_O defect increase linearly with reduction time. (d) Schematic description of electrochemical reduction process. The reaction of surface oxygen with water generates V_O ($O–Ti^{4+}–V_O$) and electrons supported from counter electrode could inject to Ti^{4+} to form Ti^{3+}.

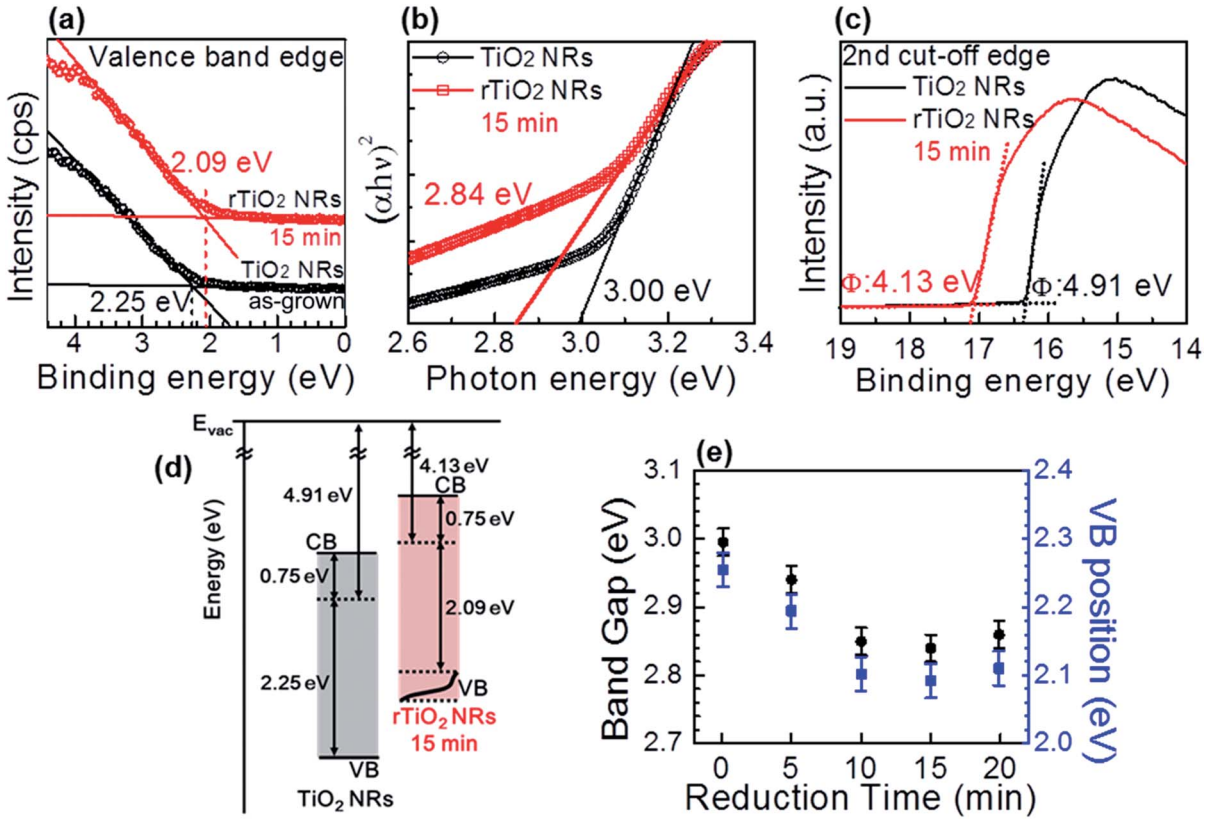

Fig. 3 (a) VB position analyzed from VB XPS spectra, (b) plots of Kubelka–Munk function *vs.* the photon energy and (c) work-function analyzed from UPS spectra of TiO_2 NRs and $rTiO_2$ NRs. (d) Schematic description of band structure of TiO_2 NRs before and after reduction. (e) Evolution of valence band and optical band gap with respect to the reduction time. After reduction for 15 min, the Fermi level was raised 0.78 eV and the VB edge is shifted up 0.16 eV to the Fermi level. The modification of the optical band gap is similar to that the VB edge.

compared to the TiO_2 NRs, the $rTiO_2$ NRs can perform better photocatalytic behavior in UV-Vis irradiation.

On the other hand, the charge recombination can affect the $rTiO_2$ NRs performance. Therefore, to avoid the recombination of photo-generated electron–hole pairs, an ultrathin layer of Pt was deposited on the $rTiO_2$ NRs by RF-magnetron sputtering. The Pt distribution on $rTiO_2$ NRs was analysed HR-TEM, as shown in Fig. 1(g) and S2.† It shows that amorphous Pt is uniformly decorated on $rTiO_2$ NRs surface with the average width and thickness are about 2.2 and 3.4 nm, respectively. Energy-dispersive X-ray spectroscopy (EDS) elementary mapping images in Fig. 1(h)–(k) show the excellent coated (almost conformal) of Pt on whole interface of exposed $rTiO_2$ NRs.

The sample was further characterized by XPS to examine the effect of the reduction process on atomic bonding in the TiO_2 NRs. The Ti $2p^{3/2}$ spectra before and after reduction are given in Fig. 2(a). The figure shows a weak peak at 456.9 eV and a strong peak at 458.3 eV, corresponding to Ti^{3+} and Ti^{4+}, respectively. The intensity of the Ti^{3+} peak increased after the reduction process, which indicates the reduction of TiO_2. The total increase was found to be 2.2%. Moreover, the change in the relative intensity of Ti^{3+} indicates the self-doping of Ti^{3+} into TiO_2 NRs.[39,50,51] The O 1s survey in Fig. 2(b) shows the presence of oxygen vacancies (V_O) at 531.0 eV, strong binding of crystalline Ti–O in TiO_2 at 529.5 eV, and weak binding of Ti and oxygen at the TiO_2 surface at 527.8 eV.[50,51] The intensity of V_O increased by 3.6% after the reduction process.

Fig. 2(c) shows the reduction time dependent formation of Ti^{3+} and V_O in $rTiO_2$ NRs, which was calculated from XPS data deconvolution shown in Fig. S3.† The Ti^{3+} was found to be saturated at an average 9.4% after a 5 min reduction time, while the V_O defects is found to be saturated at about 24% after 10 min of reduction time. This phenomenon can be explained by a reduction mechanism shown schematically in Fig. 2(d). Electrons supported from the counter electrode could inject into Ti^{4+} to form Ti^{3+}. The larger amount of electron injected into Ti^{4+} may rapidly reduce it to Ti^{3+} (saturated after 5 min reduction). Thus, the bonding of oxygen and Ti^{3+} is weaken then oxygen atoms at surface react with hydrogen ions (H^+, separated from water) to generate oxygen vacancies.

The VB position of the TiO_2 NRs and $rTiO_2$ NRs were analyzed from the VB XPS spectra, as shown in Fig. 3(a). The VB edge of TiO_2 NRs and $rTiO_2$ NRs observed at 2.25 eV and 2.09 eV, respectively, under the Fermi level, which indicates that the VB edge of the $rTiO_2$ NRs was shifted 0.16 eV to the Fermi level.[21,30] The same behavior can be observed in plots of the Kubelka–Munk function *vs.* the photon energy transformed from the total diffuse transmittance (Fig. S4†) shown in Fig. 3(b). The TiO_2 NRs reveal a band gap of 3.0 eV,[52] whereas the $rTiO_2$ NRs

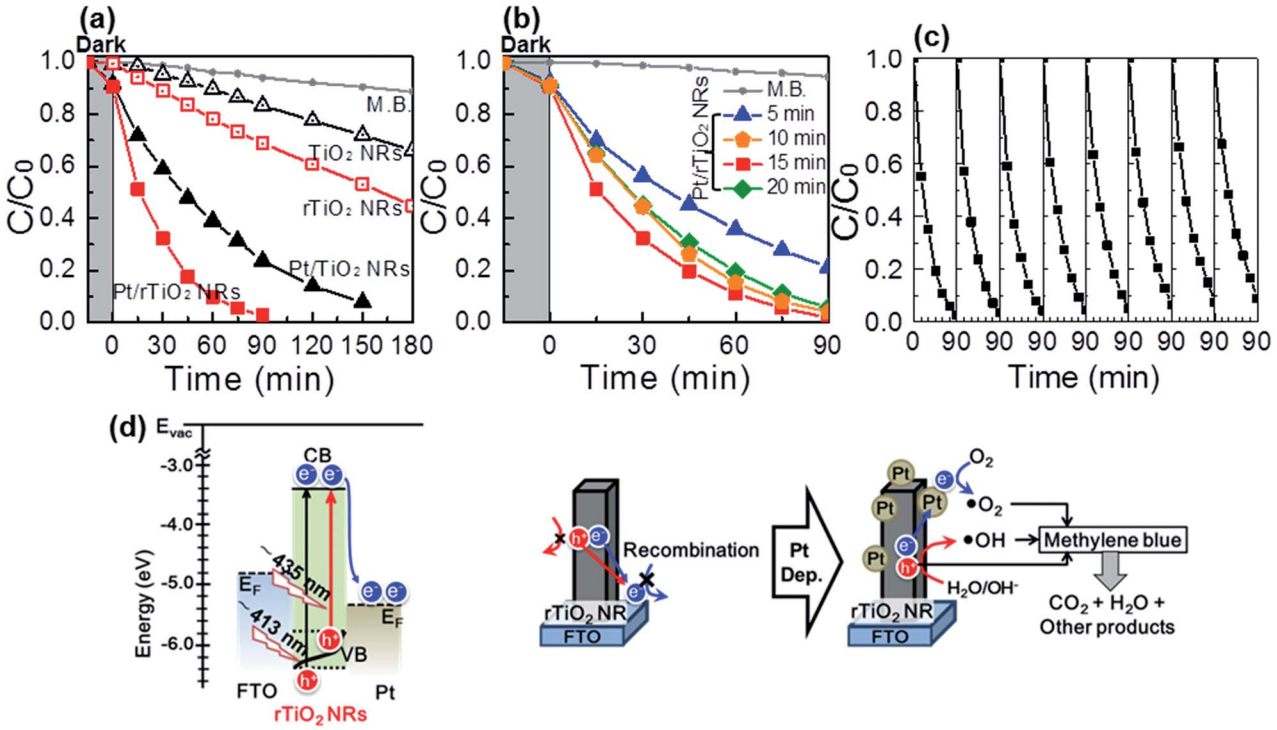

Fig. 4 (a) Photo-degradation of M.B. in TiO_2 NRs, $rTiO_2$ NRs, Pt decorated TiO_2 NRs (Pt/TiO_2 NRs) and Pt decorated $rTiO_2$ NRs (Pt/$rTiO_2$ NRs). The photocatalytic activities are enhanced after electrochemical reduction and decoration of Pt, due to the reduction of the optical band gap and recombination, respectively. (b) Photocatalytic performance of Pt decorated $rTiO_2$ NRs with different reduction times. (c) Recycled photocatalytic activities of Pt decorated $rTiO_2$ NRs. (d) Schematic description of the photocatalytic activities of Pt decorated $rTiO_2$ NRs.

exhibit an optical band gap of 2.84 eV, which is 0.16 eV lower. Fig. 3(c) shows work-function deduced from UPS spectra before and after the electrochemical reduction of TiO_2 NRs. Gap between CB and Fermi level was maintained, while the Fermi level of $rTiO_2$ NRs was raised 0.78 eV after reduction, as shown in Fig. 3(d). Therefore, reduced optical band gap of $rTiO_2$ NRs is attributed to up-shifting of VB. Every result in the UV-Vis transmittance and XPS (UPS) analysis are in well agreement. These results confirm that the surface defect in the $rTiO_2$ NRs reduce its optical band-gap by up-shifting the VB edge, which is in good agreement with previous reports.[21,30,38,51] Fig. 3(e) and S5† presents the time evolution of the VB and the tuning of the optical band gap with respect to the reduction time. Both of VB position and band gap of $rTiO_2$ NRs are found to be saturated at about 2.1 and 2.85 eV, respectively, after 10 min of reduction time. The modification of the optical band gap of the $rTiO_2$ NRs is similar to the shifted value of the VB edge to the Fermi level for all reduction times. Therefore, the reduction of the optical band-gap of $rTiO_2$ NRs by the electrochemical reduction was attributed to the modification of the VB edge.[21,30,39,53]

Fig. 4 shows the photocatalytic activities of the samples evaluated by the photo-degradation of methylene blue (M.B.) in an aqueous solution. As shown in Fig. 4(a) and S6(a),† the $rTiO_2$ NRs and Pt/$rTiO_2$ NRs show 1.48 and 12.85 times higher photocatalytic activities than that of the TiO_2 NRs and Pt/TiO_2 NRs under UV-Vis irradiation in a 180 min and 90 min reaction, respectively. This effect can be attributed to the reduction of the optical band gap. For further improvement, an ultrathin layer of Pt was deposited by RF-magnetron sputtering, as shown in Fig. 1(g). The ultrathin Pt layer can act as an electron collector, thereby reducing the charge recombination of the photogenerated electron/hole pair (e–h pair). This can enhance the overall performance. The photocatalytic activities of the Pt decorated $rTiO_2$ NRs are given in Fig. 4 and S6.† This shows that the photocatalytic activities and reaction rate constant k of Pt/$rTiO_2$ NRs (98.2% of M.B. degradation in 90 min, $k = 0.038$ min^{-1}) increased 24.3 and 9.5 fold compared with the $rTiO_2$ NRs (31.2% of M.B. degradation in 90 min, $k = 0.004$ min^{-1}).

Furthermore, the Pt-decorated $rTiO_2$ NRs also has substantial stability and cyclic endurance of the photocatalytic activities by the excellent photo-degradation of M.B. for 8 cycles, shown in Fig. 4(c). Fig. 4(b) and S6(b)† shows the photocatalytic performance of the Pt/$rTiO_2$ NRs with different electro-chemical reduction time. The results reveal that photocatalytic activities of $rTiO_2$ NRs were saturated after 10 min of reduction time. The photocatalytic behavior is in good agreement with the band structure results shown in Fig. 3(c). The rate constant k for 3 samples of 10, 15 and 20 min of reduction time are found to be similar (from 0.030 to 0.038 min^{-1}). A further reduction of the optical band gap resulted in further improvement of the photocatalytic activities.

Fig. 4(d) presents the mechanism of the enhanced photocatalytic activities of the Pt decorated $rTiO_2$ NRs. The conduction band (CB) of $rTiO_2$ NRs is located at approximately −4.4 eV under vacuum level, while the Fermi level of Pt is located under the CB of the $rTiO_2$ NRs.[54–56] Owing to the narrower band gap,

the $rTiO_2$ NRs can absorb UV to blue light in the solar spectrum to generate e–h pairs. The photo-excited electrons from $rTiO_2$ NRs tend to transfer to Pt. The ultrathin Pt collects the electrons and improves charge transfer efficiency. The photo-excited electrons trapped on Pt react with oxygen to form superoxide radicals or hydroperoxide radical to degrade M.B. The photo-excited holes located in the $rTiO_2$ NRs oxidize water to produce hydroxyl radical to oxide M.B.[57,58]

Conclusions

This study examined the optical band gap tuning of TiO_2 NRs by an electrochemical reduction method and its effects on the photocatalytic activities. The reduction process tune the optical band gap from 3.0 eV to 2.84 eV, enabling TiO_2 NRs to absorb UV to the blue light frequencies in the solar spectrum. This reduction in band gap enhanced its photocatalytic activity 1.48 fold. In addition, Pt, as an electron collector layer, was found to be another important parameter. The ultrathin Pt layer greatly reduces the e–h recombination process and can improve the photocatalytic activity significantly (24.3 fold). Moreover, the RF-magnetron sputtered TiO_2 seed layer showed much better adhesion properties than the seed layer prepared by the sol–gel method.

Acknowledgements

This research was supported by the Priority Research Centers Program (2009-0093818), the Basic Science Research Program (2015R1D1A3A03019609), and the Basic Research Lab Program (2014R1A4A1071686) through the National Research Foundation of Korea (NRF), funded by the Korean Government. This research was also supported by the "Leaders Industry-University Cooperation" Project, supported by the Ministry of Education (MOE). Y. S. Kim also thanks to Prof. S. Park and Mr J.-W. Kim of the Dep. of Physics, Pusan National University and Dr J.-S. Bae of Busan center, Korea Science Institute for the XPS analysis.

Notes and references

1 Z. Gan, X. Wu, M. Meng, X. Zhu, L. Yang and P. K. Chu, *ACS Nano*, 2014, **8**, 9304–9310.
2 A. Fakharuddin, F. D. Giacomo, A. L. Palma, F. Matteocci, I. Ahmed, S. Razza, A. D'Epifanio, S. Licoccia, J. Ismail, A. D. Carlo, T. M. Brown and R. Jose, *ACS Nano*, 2015, **9**, 8420–8429.
3 Y. Dou, S. Zhang, T. Pan, S. Xu, A. Zhou, M. Pu, H. Yan, J. Han, M. Wei, D. G. Evans and X. Duan, *Adv. Funct. Mater.*, 2015, **25**, 2243–2249.
4 B. Qiu, M. Xing and J. Zhang, *J. Am. Chem. Soc.*, 2014, **136**, 5852–5855.
5 J.-Y. Zheng, S.-H. Bao, Y. Guo and P. Jin, *ACS Appl. Mater. Interfaces*, 2014, **6**, 5940–5946.
6 J. Tao, M. Yang, J. W. Chai, J. S. Pan, Y. P. Feng and S. J. Wang, *J. Phys. Chem. C*, 2014, **118**, 994–1000.
7 Z. Zhan, J. An, H. Zhang, R. V. Hansen and L. Zheng, *ACS Appl. Mater. Interfaces*, 2014, **6**, 1139–1144.
8 I. S. Cho, M. Logar, C. H. Lee, L. Cai, F. B. Prinz and X. Zheng, *Nano Lett.*, 2014, **14**, 24–31.
9 S. N. R. Inturi, T. Boningari, M. Suidan and P. G. Smirniotis, *J. Phys. Chem. C*, 2014, **118**, 231–242.
10 S. Padikkaparambil, Z. Yaakob, B. N. Narayanan, R. Ramakrishnan and S. Viswanathan, *J. Sol-Gel Sci. Technol.*, 2012, **63**, 108–115.
11 J. Biedrzycki, S. Livraghi, E. Giamello, S. Agnoli and G. Granozzi, *J. Phys. Chem. C*, 2014, **118**, 8462–8473.
12 R. Asahi, T. Morikawa, T. Ohwaki, K. Aoki and Y. Taga, *Science*, 2001, **293**, 269–271.
13 A. Kumar and T. Mohanty, *J. Phys. Chem. C*, 2014, **118**, 7130–7138.
14 R. Asahi, T. Morikawa, H. Irie and T. Ohwaki, *Chem. Rev.*, 2014, **114**, 9824–9852.
15 Z. Jiang, Y. Tang, Q. Tay, Y. Zhang, O. I. Malyi, D. Wang, J. Deng, Y. Lai, H. Zhou, X. Chen, Z. Dong and Z. Chen, *Adv. Energy Mater.*, 2013, **3**, 1368–1380.
16 M.-Z. Ge, C.-Y. Cao, S.-H. Li, Y.-X. Tang, L.-N. Wang, N. Qi, J.-Y. Huang, K.-Q. Zhang, S. S. Al-Deyabe and Y.-K. Lai, *Nanoscale*, 2016, **8**, 5226–5234.
17 Y.-C. Pu, G. Wang, K.-D. Chang, Y. Ling, Y.-K. Lin, B. C. Fitzmorris, C.-M. Liu, X. Lu, Y. Tong, J. Z. Zhang, Y.-J. Hsu and Y. Li, *Nano Lett.*, 2013, **13**, 3817–3823.
18 Y. Tang, Z. Jiang, G. Xing, A. Li, P. D. Kanhere, Y. Zhang, T. C. Sum, S. Li, X. Chen, Z. Dong and Z. Chen, *Adv. Funct. Mater.*, 2013, **23**, 2932–2940.
19 M. Ge, Q. Li, C. Cao, J. Huang, S. Li, S. Zhang, Z. Chen, K. Zhang, S. S. Al-Deyab and Y. Lai, *Adv. Sci.*, 2016, **3**, 1600152.
20 S. Liu, J. Yu and W. Wang, *Phys. Chem. Chem. Phys.*, 2010, **12**, 12308–12315.
21 A. Naldoni, M. Allieta, S. Santangelo, M. Marelli, F. Fabbri, S. Cappelli, C. L. Bianchi, R. Psaro and V. D. Santo, *J. Am. Chem. Soc.*, 2012, **134**, 7600–7603.
22 G. R. Torres, T. Lindgren, J. Lu, C.-G. Granqvist and S.-E. Lindquist, *J. Phys. Chem. B*, 2004, **108**, 5995–6003.
23 J. Wang, D. N. Tafen, J. P. Lewis, Z. Hong, A. Manivannan, M. Zhi, M. Li and N. Wu, *J. Am. Chem. Soc.*, 2009, **131**, 12290–12297.
24 X. Chen, L. Liu and F. Huang, *Chem. Soc. Rev.*, 2015, **44**, 1861–1885.
25 Z. Zhang, X. Yang, M. N. Hedhili, E. Ahmed†, L. Shi and P. Wang, *ACS Appl. Mater. Interfaces*, 2014, **6**, 691–696.
26 J. Chen, W. Song, H. Hou, Y. Zhang, M. Jing, X. Jia and X. Ji, *Adv. Funct. Mater.*, 2015, **25**, 6793–6801.
27 H. Zhou and Y. Zhang, *J. Phys. Chem. C*, 2014, **118**, 5626–5636.
28 B. Qiu, Y. Zhou, Y. Ma, X. Yang, W. Sheng, M. Xing and J. Zhang, *Sci. Rep.*, 2015, **5**, 8591.
29 F. Zuo, L. Wang, T. Wu, Z. Zhang, D. Borchardt and P. Feng, *J. Am. Chem. Soc.*, 2010, **132**, 1856–11857.
30 Q. Kang, J. Cao, Y. Zhang, L. Liu, H. Xu and J. Ye, *J. Mater. Chem. A*, 2013, **1**, 5766–5774.
31 J. M. Macak, B. G. Gong, M. Hueppe and P. Schmuki, *Adv. Mater.*, 2007, **19**, 3027–3031.

32 X. Chen, L. Liu, P. Y. Yu and S. S. Mao, *Science*, 2011, **331**, 746–750.
33 J. E. Rekoske and M. A. Barteau, *J. Phys. Chem. B*, 1997, **101**, 1113–1124.
34 J.-Y. Shin, J. H. Joo, D. Samuelis and J. Maier, *Chem. Mater.*, 2012, **24**, 543–551.
35 H. He, K. Yang, N. Wang, F. Luo and H. Chen, *J. Appl. Phys.*, 2013, **114**, 213505.
36 S.-T. Myung, M. Kikuchi, C. S. Yoon, H. Yashiro, S.-J. Kim, Y.-K. Sun and B. Scrosati, *Energy Environ. Sci.*, 2013, **6**, 2609–2614.
37 B. Liu and E. S. Aydil, *J. Am. Chem. Soc.*, 2009, **131**, 3985–3990.
38 C. Xu, Y. Song, L. Lu, C. Cheng, D. Liu, X. Fang, X. Chen, X. Zhu and D. Li, *Nanoscale Res. Lett.*, 2013, **8**, 391.
39 Z. Zhang, M. N. Hedhili, H. Zhu and P. Wang, *Phys. Chem. Chem. Phys.*, 2013, **15**, 15637–15644.
40 H. Li, Z. Chen, C. K. Tsang, Z. Li, X. Ran, C. Lee, B. Nie, L. Zheng, T. Hung, J. Lu, B. Pan and Y. Y. Li, *J. Mater. Chem. A*, 2014, **2**, 229–236.
41 X. Feng, K. Zhu, J. Frank, C. A. Grimes and T. E. Mallouk, *Angew. Chem.*, 2012, **124**, 2781–2784.
42 H. S. Jung, J.-K. Lee, J. Lee, B. S. Kang, Q. Jia, M. Nastasi, J. H. Noh, C.-M. Cho and S. H. Yoon, *Langmuir*, 2008, **24**, 2695–2698.
43 S. Takedaa, S. Suzukia, H. Odakaa and H. Hosonob, *Thin Solid Films*, 2001, **392**, 338–344.
44 M. Yamagishi, S. Kuriki, P. K. Song and Y. Shigesato, *Thin Solid Films*, 2003, **442**, 227–231.
45 I. S. Cho, Z. Chen, A. J. Forman, D. R. Kim, P. M. Rao, T. F. Jaramillo and X. Zheng, *Nano Lett.*, 2011, **11**, 4978–4984.
46 P. Ballirano and R. Caminiti, *J. Appl. Crystallogr.*, 2001, **34**, 757–762.
47 W. J. Howard, *Crystal Chemistry and Refractivity*, Cambridge University, Cambridge, UK, 1988.
48 P. B. Allen, *Nano Lett.*, 2007, **7**, 6–10.
49 A. Kumar, A. R. Madaria and C. Zhou, *J. Phys. Chem. C*, 2010, **114**, 7787–7792.
50 B. Santara, P. K. Giri, K. Imakita and M. Fujii, *J. Phys. Chem. C*, 2013, **117**, 23402–23411.
51 M. C. Biesinger, L. W. M. Lau, A. R. Gerson and R. S. C. Smart, *Appl. Surf. Sci.*, 2010, **257**, 887–898.
52 J.-J. Wu and C.-C. Yu, *J. Phys. Chem. B*, 2004, **108**, 3377–3379.
53 X. Chen, L. Liu, P. Y. Yu and S. S. Mao, *Science*, 2011, **331**, 746–750.
54 W.-N. Wang, W.-J. An, B. Ramalingam, S. Mukherjee, D. M. Niedzwiedzki, S. Gangopadhyay and P. Biswas, *J. Am. Chem. Soc.*, 2012, **134**, 11276–11281.
55 H. Chen, S. Chen, X. Quan, H. Yu, H. Zhao and Y. Zhang, *J. Phys. Chem. C*, 2008, **112**, 9285–9290.
56 Y.-C. Chen, Y.-C. Pu and Y.-J. Hsu, *J. Phys. Chem. C*, 2012, **116**, 2967–2975.
57 S. Lakshmi, R. Renganathan and S. Fujita, *J. Photochem. Photobiol., A*, 1995, **88**, 163–167.
58 A. Houas, H. Lachheb, M. Ksibi, E. Elaloui, C. Guillard and J.-M. Herrmann, *Appl. Catal., B*, 2001, **31**, 145–157.